Polar Science 47 (2026) 101303

Contents lists available at ScienceDirect

Polar Science

journal homepage: www.elsevier.com/locate/polar

Variations in aerosol composition inferred from metal concentrations in the SE-Dome ice core, southeastern Greenland

Nao Esashi [a,c,*], Chiaki Sasaki [b], Toshitaka Suzuki [b], Motohiro Hirabayashi [c], Yoshinori Iizuka [d], Sumito Matoba [d], Koji Fujita [a]

[a] Graduate School of Environmental Studies, Nagoya University, Nagoya, Japan
[b] Faculty of Science, Yamagata University, Yamagata, Japan
[c] National Institute of Polar Research, Tachikawa, Japan
[d] Institute of Low Temperature Science, Hokkaido University, Sapporo, Japan

A B S T R A C T

The insoluble fraction of aerosols is typically quantified as the dust concentration, but its elemental composition remains poorly characterized, whereas the soluble fraction is commonly measured as the ion concentration. Analyzing the elemental composition of the insoluble fraction is crucial for identifying aerosol sources and understanding the factors that drive their variability. This study investigates temporal variations in total (i.e., soluble and insoluble) metal concentrations in an ice core from the southeastern dome of Greenland, covering the period from 1957 to 2014. Crustal elements (Al, non-sea salt (nss) Ca, and Fe) exhibited high concentrations during 1957–1975 (Period 1), low concentrations during 1976–1999 (Period 2), and a subsequent increase after 2000 (Period 3). The elemental ratios and seasonal flux patterns suggest that the aerosol sources and the factors controlling aerosol concentrations varied among the periods. Periods 1 and 2 are influenced by long-range transport of Asian mineral dust and anthropogenic emissions from North America and Europe, whereas Period 3 reflects growing contributions from local Greenland sources. Period 3 can be further divided into two periods: Period 3a (2000–2007) and Period 3b (2008–2014), based on differences in their compositions. During Period 3a, the enrichment in nssCa likely reflects increased inputs of soluble nssCa from coastal meltwater streams, along with additional contributions from the weathering of newly exposed carbonate rocks. In Period 3b, local Greenland soils became the dominant source, reducing the influence of Asian dust. Elevated Fe levels suggest additional contributions from volcanic soils, possibly from Iceland.

1. Introduction

Greenland ice cores have been extensively used to investigate the long-term variability in the composition and sources of atmospheric aerosols. Metal components in ice cores exist in both soluble and insoluble forms. Ice cores and snow samples are typically melted before analysis, and soluble fractions of aerosol components are commonly measured via ion chromatography (IC) or continuous flow analysis (CFA) after dissolution in water. The soluble fraction of aerosol compositions in many Greenland ice cores has been investigated, with each ion serving as a tracer for its respective source. For example, Ca^{2+} traces mineral dust, Na^{+} and Cl^{-} reflect sea salt, NH_4^{+} and K^{+} indicate biomass burning, and SO_4^{2-} serves as a tracer for anthropogenic emissions as well as volcanic activity and biogenic sources (Legrand and Mayewski, 1997; Dibb et al., 2007; Kuramoto et al., 2011; Oyabu et al., 2016; Nakazawa et al., 2021). However, this approach can be limited in the amount and robustness of information that can be obtained. For example, the relationship between Ca^{2+} and mineral dust depends on its solubility, origin, mineralogy, and coexisting components (Ruth et al., 2002, 2008; Banta et al., 2008; Lai et al., 2017).

The number, mass, and size distribution of the particles in the insoluble fraction are measured as the dust concentration. Deep ice cores from inland Greenland show that dust concentrations are closely correlated with temperature and are 10–100 times higher during glacial periods than during interglacial periods (Steffensen, 1997; Ruth et al., 2002; Schüpbach et al., 2018). Recent studies have indicated an increase in dust from coastal Greenland, associated with ongoing warming (Amino et al., 2021; Kjær et al., 2022). Dust particle size is frequently used as an indicator of transport distance, in combination with backward trajectories and meteorological data, to identify its sources. In some cases, aerosol sources have been identified by comparing Sr, Nd, and Pb isotope ratios or mineral compositions with reference data (e.g., Bory et al., 2003a, 2003b; Lupker et al., 2010; Nagatsuka et al., 2021). However, in many other cases, the elemental composition of insoluble particles is not available, necessitating the indirect inference of sources.

Efforts have been made to characterize the composition of the

* Corresponding author. Graduate School of Environmental Studies, Nagoya University, Nagoya, Japan.
E-mail address: esashi.nao@nipr.ac.jp (N. Esashi).

https://doi.org/10.1016/j.polar.2025.101303
Received 21 July 2025; Received in revised form 14 October 2025; Accepted 24 October 2025
Available online 30 October 2025

insoluble fraction. For example, metal components in filter-captured particles from the Dome C ice core drilled in Antarctica were measured via particle-induced X-ray emission (PIXE; Ghermandi et al., 2003; Marino et al., 2004) and acid dissolution followed by mass analysis via inductively coupled plasma–sector field mass spectrometry (ICP-SFMS; Gaspari et al., 2006). These studies indicate that many metal components are predominantly found in the insoluble fraction. In particular, metal components derived from crustal dust, such as Al and Fe, are less soluble (Gaspari et al., 2006; Lai et al., 2017). Therefore, measurements of the insoluble fraction are essential for understanding the compositions of crustal origin aerosols (Sato et al., 2013). Currently, such measurements have been attempted in Greenland snow samples, but they are limited to two sites in the northwest coastal region and the northeast inland region and cover only the last few years (Lai et al., 2017; Komuro et al., 2024).

An ice core 90.45 m deep was drilled at the SE-Dome site in southeastern Greenland in May 2015 (Iizuka et al., 2016). This area is a high accumulation zone, with an accumulation rate of 1.01 ± 0.22 m water eq. yr^{-1} (1960–2014; Iizuka et al., 2017). Cores recovered from high-accumulation sites do not reach great ages; however, their high temporal resolution and reduced effects from chemical alteration at the snow surface enable the strong preservation of their chemical signals (Iizuka et al., 2017, 2018; Wei et al., 2025). The SE-Dome core can be precisely dated, with an uncertainty of approximately ±1 month (Furukawa et al., 2017). During ice core extraction, a 3.55 m deep snow pit was also excavated, allowing for the observation of seasonal variations in water isotope ratios and major ion concentrations (Oyabu et al., 2016). The high temporal resolution and strong chemical preservation of the SE-Dome core enable a wide range of proxy analyses. Iizuka et al. (2018) reconstructed major ion fluxes and reported that the non–sea salt SO_4^{2-} flux from the SE-Dome core (1970–2010) closely corresponded to anthropogenic SOx emissions from North America. Iizuka et al. (2022) analyzed sulfate aerosols extracted by sublimation and demonstrated a significant decline in particles smaller than 0.4 μm after 2010–2012, following the implementation of emission controls after a period of high anthropogenic emissions (1973–1975). Furthermore, Miyamoto et al. (2022) used X-ray absorption near-edge structure (XANES) data to show that Ca in ice cores predominantly occurred as calcite ($CaCO_3$) during the 1970s–1980s but as gypsum ($CaSO_4 \bullet 2H_2O$) during the 1990s–2000s. This change in form suggests that atmospheric SO_2 reacts with dust particles containing calcite, originating from East Asia, to form gypsum. Amino et al. (2021) analyzed the number, mass, and size distribution of dust particles in the SE-Dome core and reported higher dust concentrations and a greater fraction of coarse particles after 2000, likely reflecting the expansion of snow-free areas along the Greenland coastline due to ongoing warming, which contributed additional local dust.

These proxy data enable the reconstruction of paleoenvironmental conditions at the SE-Dome over the past 60 years; however, some details are inconsistent. For example, the Ca^{2+} in SE-Dome snow pit samples is predominantly derived from terrestrial dust and reaches a maximum in spring (Oyabu et al., 2016), whereas the dust mass flux in the SE-Dome ice core peaks in autumn after 2000 (Amino et al., 2021). Furthermore, although Miyamoto et al. (2022) suggested that Ca in the SE-Dome ice core originates from East Asian calcite, backward trajectory analysis reveals little contribution from Asia (Iizuka et al., 2018). Analyzing both soluble and insoluble fractions may help resolve these uncertainties and enable a more comprehensive understanding of aerosol compositions.

In this study, we reconstructed total metal concentrations in the SE-Dome ice core over the past 60 years. This approach enables a quantitative evaluation of aerosol compositions, including both soluble and insoluble fractions. Analyzing their temporal trends and seasonal variations at 10–to 20-year intervals helps complement and strengthen previously derived information from ion and dust data, thereby providing a more comprehensive view of the variation in aerosol composition.

2. Material and methods

2.1. Ice core samples and age scale

In this study, we used an ice core drilled to a depth of 90.45 m at the SE-Dome site (67.18°N, 36.37°W, 3170 m above sea level) in southeastern Greenland. The annual mean temperature at SE-Dome is −20.9 °C, based on firn temperature measurements at a 20 m depth (Iizuka et al., 2017). The SEIS2016 age scale, constructed using oxygen isotope matching for the period 1960–2014, was used for ice core dating (Furukawa et al., 2017). The SEIS2016 age scale was carefully evaluated against independent dating markers, including tritium and volcanic events, with an accuracy of within two months. For 1957–1959, maximum Na^+ concentrations were used as depth markers for February precipitation, and ages were determined by linear interpolation (Iizuka et al., 2018).

2.2. Total metal concentration measurement

Ice core samples were cut at 50 mm depth intervals in a −20 °C cold room at the Institute of Low Temperature Science, Hokkaido University. The outer 5 mm of each sample was removed with a clean ceramic knife to eliminate contamination, and the samples were placed in clean polyethylene bags. The samples, which were kept frozen at −20 °C after being transported to Yamagata University, were melted at room temperature before analysis. Inside a Class 100 clean bench, the melted samples were transferred to perfluoroalkoxy alkane (PFA) containers (DV-7, San-ai Kagaku) and placed in a chamber on a ceramic hot plate at 180 °C to evaporate to dryness. After complete evaporation, 0.3 mL nitric acid and 0.2 mL hydrofluoric acid were added to the residues in the PFA containers, which were then placed in pressure decomposition vessels (P-25, San-ai Kagaku) and heated in a microwave oven at 200 W for 15 min to dissolve the residues. The samples were subsequently heated again on a hot plate to evaporate to dryness. After complete evaporation, 0.1 mL of nitric acid was added to dissolve the residues, and the solution was transferred to centrifuge tubes (SuperClear Tubes with Plug Seal Cap, Labcon) and diluted to 10 mL with ultrapure water (18.2 MΩ cm). All PFA containers and centrifuge tubes were cleaned by soaking in 1 N nitric acid overnight to remove metal contamination. The detailed methods for dissolving the insoluble fraction are described by Suzuki and Sensui (1991).

The concentrations of Na, Al, Ca, and Fe were measured via ICP−MS (7700, Agilent Technologies) at the National Institute of Polar Research. Sample concentrations were determined using calibration curves prepared from standard solutions (XSTC-13, SPEX). Procedural blanks were also measured and subtracted from the results. The relative standard error was within 5 %. Measurements were conducted on 717 samples collected at 50 mm depth intervals from the 90.45 m ice core, with some gaps in the measurement intervals (Fig. 1).

2.3. Estimation of the non-sea salt fraction

Among the four measured elements, Al and Fe are mainly crustal, whereas Na and Ca are also derived from sea salt. Assuming that all the Al originates from the crust, the sea salt fraction (ss) and crustal non-sea salt fraction (nss) of Na were first calculated using the following equations:

$$[\text{nssNa}] = (\text{Na/Al})_{\text{crust}} \times [\text{t-Al}]$$

$$[\text{ssNa}] = [\text{t-Na}] - [\text{nssNa}]$$

Here, [t-Na] is the total concentration of Na, and $(\text{Na/Al})_{\text{crust}}$ is the average crustal composition ratio of Na to Al, which is 0.287 (Taylor, 1964). Using [ssNa], the non-sea salt fraction of Ca was calculated as follows:

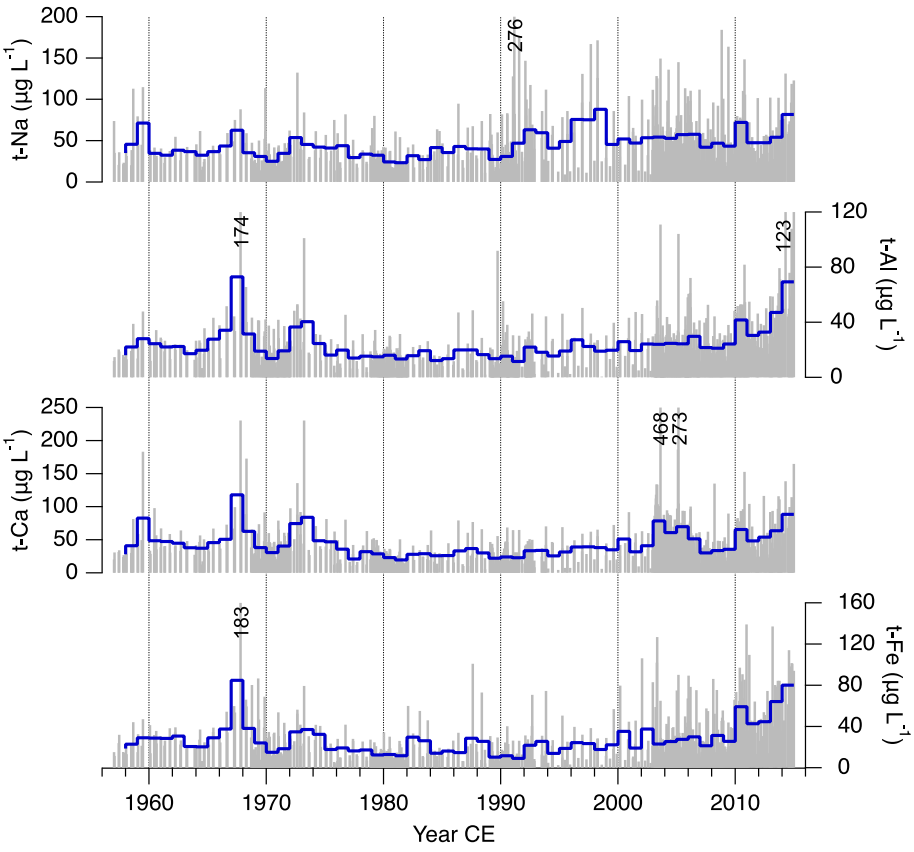

Fig. 1. Time series of total metal concentrations in the SE-Dome ice core from 1957 to 2014 CE. The blue line indicates the annual average, and the gray bars indicate the concentration for each measured sample. The values indicate overshoot spikes in concentration (μg L^{-1}). (For interpretation of the references to colour in this figure legend, the reader is referred to the Web version of this article.)

$$[\text{t-nssCa}] = [\text{t-Ca}] - (\text{Ca/Na})_{\text{sea}} \times [\text{ssNa}]$$

where $(\text{Ca/Na})_{\text{sea}} = 0.022$ is the average seawater composition ratio (Broecker and Peng, 1982). In this study, total concentrations are indicated by a "t-" prefix (e.g., t-Ca) to distinguish them from ion concentrations.

3. Results & discussion

3.1. General characteristics of total metal concentrations

The average total concentrations of the four measured elements are shown in Table 1. Among them, t-Na and t-Ca had the highest concentrations. Elevated Na^+ concentrations have also been reported in snow pit samples from SE-Dome, likely due to its proximity to the coastline (Oyabu et al., 2016). The high t-Na concentration observed in this study similarly suggests a substantial contribution from sea salt. Among the four elements, Na and Ca are derived from both sea salt and continental sources. After removing the sea salt fraction, the average non–sea salt concentrations were 7.0 ± 6.8 μg L^{-1} for nssNa and 43.9 ± 36.1 μg L^{-1} for nssCa. The average proportions of the non–sea salt fractions relative to the total concentrations were 15.3 % for Na and 96.3 % for Ca. These results indicate that Na in the SE-Dome core is primarily of marine origin, whereas Ca is mainly of continental origin.

Fig. 1 shows the time series of total metal concentrations (t-Na, t-Al, t-Ca, and t-Fe) from 1957 to 2014. The variation patterns of t-Al, t-Ca, and t-Fe are highly consistent, with concentration peaks in the late 1960s to early 1970s and after 2000. A clear increasing trend is evident after 2000. In contrast, t-Na concentrations were elevated in the early 1990s, marking the highest levels observed during the past 60 years.

Table 2 presents the correlation coefficients among the total concentrations of the four elements. All four elements exhibit relatively strong positive correlations ($r > 0.57$), with the highest correlation observed between t-Fe and t-Al ($r = 0.85$). These results indicate that aerosols containing these elements likely originated from similar sources and were transported to the SE-Dome during comparable periods via similar pathways.

3.2. Comparison of trends in total metals and dust

Ca in Arctic snow is generally considered to be derived from sea spray or mineral dust, and nssCa, after correction for marine contributions, is frequently used as a proxy for dust concentration (de Caritat et al., 2005; Dibb et al., 2007; Krnavek et al., 2012). In the SE-Dome core, non–sea salt fractions account for 96.3 % of the total Ca,

Table 1
Average values and standard deviations of total metal concentrations in all measured samples (μg L^{-1}).

	t-Na	t-Al	t-Ca	t-Fe
Average ± 1σ	45.7 ± 30.7	24.4 ± 23.6	44.8 ± 36.4	26.7 ± 26.4

Table 2
Correlation coefficients among the total concentrations of four elements (t-Na, t-Al, t-Ca, and t-Fe) measured from the SE-Dome ice core (n = 694). All the correlations are statistically significant ($p < 0.001$).

	t-Na	t-Al	t-Ca	t-Fe
t-Na	1	0.58	0.61	0.57
t-Al		1	0.75	0.85
t-Ca			1	0.66
t-Fe				1

indicating a limited contribution from sea spray. To investigate the relationships with other crustal elements and dust, nssCa concentrations were used in subsequent analyses. In addition to nssCa, the elemental concentrations of Al and Fe in ice cores are commonly used as proxies for terrestrial dust (e.g., Whitlow et al., 1992; Drab et al., 2002). Because these elements are predominantly contained in insoluble dust, we evaluated their relationships by comparing the concentrations of t-Al, t-nssCa, t-Fe, and dust in the SE-Dome core. The mass concentration of dust in the SE-Dome core was previously reported by Amino et al. (2021). However, these values were derived by converting particle volumes measured by a Coulter Counter, assuming a constant density. Consequently, they are not directly comparable with total metal concentrations. To facilitate comparison, we normalized the annual average concentrations of t-Al, t-nssCa, t-Fe, and dust to their respective entire-period average values and assessed their variation trends (Fig. 2). The variation patterns of the total concentrations of the three crustal elements are similar, with maximum values occurring in 1967. While high concentrations above the average frequently appear during 1960–1975 and after 2000, few such cases are observed during 1976–1999; in particular, t-nssCa remained below its average during this period. The variation in dust concentration broadly followed the pattern of total concentrations, with higher-than-average values after 2000. However, during 1960–1975, the dust concentration was only slightly above the average and did not reach more than twice the average, in contrast to the total concentrations. Based on these variation patterns, we divided the data into three periods: Period 1 (1957–1975), Period 2 (1976–1999), and Period 3 (2000–2014), for further discussion of their respective variation mechanisms.

To further assess the variation trends, correlation coefficients were calculated between the dust concentration and the total concentrations of three elements (t-Al, t-nssCa, and t-Fe) (Table 3). Over the entire period (1960–2014), dust showed moderate positive correlations with the three elements (r = 0.52–0.58). When analyzed by period, no significant correlations were found in Period 1, and only weak correlations

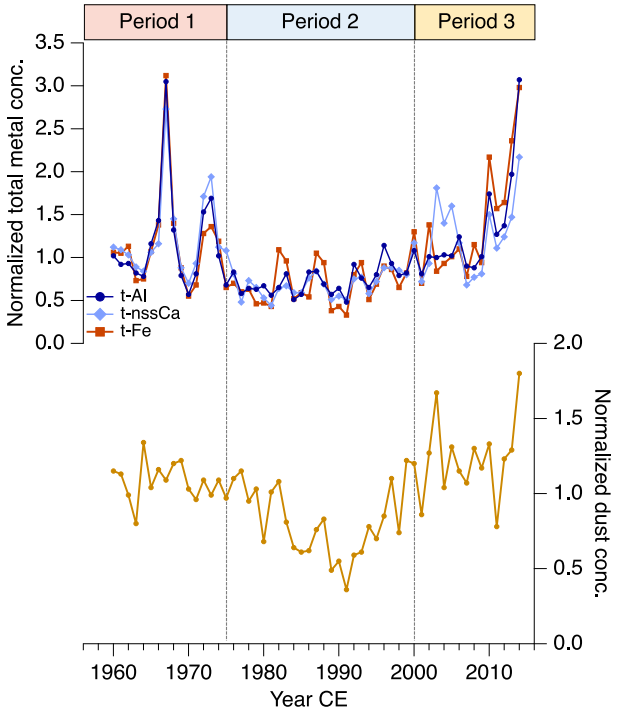

Fig. 2. Temporal trends of normalized t-Al, t-nssCa, t-Fe, and dust mass concentrations in the SE-Dome ice core. Each variable is scaled to its mean over the entire period (1960–2014, with a mean of 1). The dust mass concentrations are from Amino et al. (2021).

Table 3
Correlation between dust mass and total concentrations by period. Correlation coefficients are shown between dust mass concentration (particle size range 0.6–18 μm; Amino et al., 2021) and total concentrations of t-Al, t-nssCa, and t-Fe in the SE-Dome core for each period. The sample size (number of years) for each period is indicated by n.

	t-Al	t-nssCa	t-Fe	n
Period 1 (1960–1975)	0.07^{+}	0.01^{+}	0.14^{+}	16
Period 2 (1976–1999)	0.21^{+}	0.29^{+}	0.35^{+}	24
Period 3 (2000–2014)	$0.58^{\#}$	0.73*	0.49^{+}	15
Period 3a (2000–2007)	0.30^{+}	$0.76^{\#}$	0.23^{+}	8
Period 3b (2008–2014)	0.75^{+}	0.70^{+}	0.66^{+}	7
All Periods (1960–2014)	0.52	0.58	0.56	55

$^{+}$ $p > 0.05$, $^{\#}$ $0.05 > p > 0.01$, * $0.01 > p > 0.001$, no remark $p < 0.001$.

appeared in Period 2 (r = 0.21–0.35). In contrast, Period 3 showed moderate to strong positive correlations (r > 0.49), with the strongest correlation observed for t-nssCa (r = 0.73). Although some correlations were not statistically significant ($p > 0.05$), the overall trend indicates a progressive increase in correlation strength over time. This suggests that the sources, transport pathways, and deposition processes influencing both dust and total metal concentrations have become increasingly similar in recent decades.

3.3. Period-based differences in aerosol composition and seasonality

Distinct temporal trends were observed between dust and total concentrations, suggesting that aerosol composition varied across the three periods. In Period 1, the total concentrations of crustal elements were up to three times higher than the average, whereas the dust concentrations increased by only approximately 1.3 times. Moreover, the timing of peak concentrations did not coincide between the two (Fig. 2). To further investigate these period-specific differences in aerosol composition, we examined the relationship between total and ion concentrations, along with the variation in elemental ratios within the total concentrations.

Ion concentrations in the SE-Dome core were measured by Iizuka et al. (2018), and annual fluxes were calculated as the product of the annual mean concentration and accumulation rate. In this study, we focused on Ca, for which both total and ion concentrations were available. Iizuka et al. (2018) also calculated the non–sea salt Ca^{2+} ($nssCa^{2+}$) flux and used it as a dust proxy. We calculated the flux of t-nssCa by multiplying the concentration by the accumulation rate and compared its temporal trend with that of $nssCa^{2+}$. Fig. 3 shows the annual fluxes of t-nssCa and $nssCa^{2+}$ in the SE-Dome core from 1957 to 2014. The t-nssCa flux increased during Periods 1 and 3, whereas the $nssCa^{2+}$ flux remained nearly constant from 1957 to 2000 and increased thereafter (Iizuka et al., 2018). Assuming that $nssCa^{2+}$ represented the entire soluble fraction, we estimated the solubility of nssCa by dividing the ion concentration by the total concentration (Fig. 3). The average solubility over the entire period was 10.6 %, but it varied considerably, ranging from 3.2 % to 34.4 %. A comparison of periods with high total concentrations revealed that the solubility was lower in Period 1 (7.0 %) than in Period 3 (12.4 %). In Period 2, both the total and ion concentrations were low, resulting in a relatively high average solubility of 12.3 %. Although studies comparing t-Ca, including its insoluble fraction, with Ca^{2+} concentrations in Greenland snow samples are limited, a few examples have been reported. Lai et al. (2017) reported an average Ca solubility of 70.6 ± 34.9 % in snow samples from multiple sites in northwestern Greenland. Komuro et al. (2024) analyzed nssCa in snow from an inland site in northeastern Greenland (EGRIP) and observed substantial seasonal variation, with solubility approaching 100 % from winter to spring. In contrast, the average solubility of nssCa in the SE-Dome core was 10.6 %, which was considerably lower than that reported in these previous studies. This result reflected much higher total

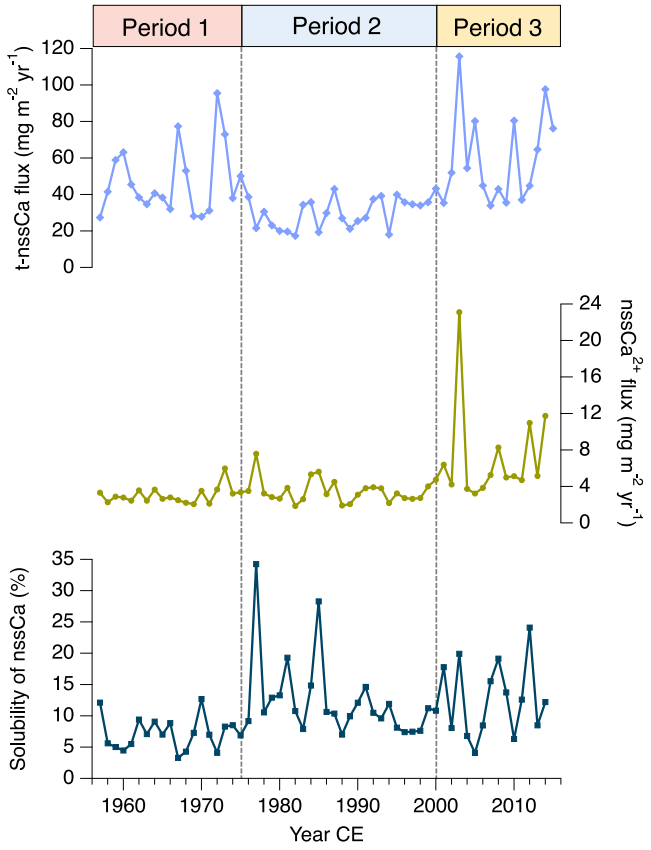

Fig. 3. Annual mean t-nssCa and nssCa^{2+} fluxes and nssCa solubility in the SE-Dome core (1957–2014). The nssCa^{2+} flux data are from Iizuka et al. (2018).

Ca concentrations relative to the ion concentrations. The discrepancy was attributed to several factors, including differences in sampling locations within Greenland, analytical methods used to measure total concentrations, and the ages of the samples. Coastal sites in Greenland are known to exhibit higher dust fluxes than inland areas (Bory et al., 2003b; Amino et al., 2021), and their proximity to exposed, snow-free terrain near the ice sheet margin likely contributes to increased input of insoluble aerosols. Furthermore, total concentration measurements require dissolution of insoluble particles, and the dissolution methods differ among studies, potentially resulting in varying recovery rates of the insoluble fraction. In addition, the previous studies referenced above are based on snow samples collected after 2010, whereas the SE-Dome core provides an average over the past 60 years. These temporal differences may also contribute to the observed variability in solubility. Thus, multiple complex factors likely underlie the differences in Ca solubility among sites.

The correlation coefficient between the annual fluxes of t-nssCa and nssCa^{2+} in the SE-Dome core over the entire period was r = 0.55 ($p < 0.001$), indicating a moderate positive relationship. When analyzed by period, the correlations were as follows: Period 1, r = 0.35 ($p > 0.05$); Period 2, r = 0.09 ($p > 0.05$); and Period 3, r = 0.64 ($p < 0.01$), with the strongest correlation observed in Period 3. This suggests that during Period 3 in particular, t-nssCa and nssCa^{2+} exhibited similar temporal patterns and were likely influenced by common transport processes. These findings, together with the comparison between total and ionic components, further support the interpretation that aerosol composition varied across the three periods.

We compared the concentration ratios of crustal elements (t-Al, t-nssCa, and t-Fe). The ternary diagram in Fig. 4 shows the ratios of each element to their total sum (100 %), with points closer to a corner indicating higher proportions of that element. Period 1 (t-Al: 5–40 %, t-nssCa: 32–88 %, t-Fe: 6–46 %) shows enrichment in t-nssCa. Period 2 (t-Al: 5–62 %, t-nssCa: 27–85 %, t-Fe: 10–58 %) largely overlaps with Period 1 but shows a relative increase in t-Al and t-Fe due to lower t-nssCa. In Period 3 (t-Al: 10–42 %, t-nssCa: 20–81 %, t-Fe: 7–67 %), both t-nssCa and t-Fe are enriched, whereas t-Al is low. Furthermore, the elemental ratios within Period 3 shifted after 2008. From 2000 to 2007 (Period 3a), many samples are rich in t-nssCa, but after 2008 (Period 3b), none show t-nssCa >60 %. Instead, several samples present t-Fe > 50 % alongside low t-nssCa. These results highlight differences in elemental compositions among periods, as well as a change within Period 3 after 2008. The mechanisms responsible for these variations in aerosol composition are discussed in Section 3.4.

Previous studies have demonstrated that the chemical components in Greenland snow and ice cores exhibit distinct seasonal patterns (e.g., Legrand and Mayewski, 1997; Oyabu et al., 2016; Iizuka et al., 2018). To assess the seasonal variability in crustal aerosols, we analyzed the seasonal trends of t-Al, t-nssCa, and t-Fe in the SE-Dome core. The seasonal mean fluxes were calculated by multiplying the seasonal mean total concentrations by the corresponding seasonal accumulation rates, allowing for comparison with the dust flux from the SE-Dome core reported by Amino et al. (2021). Spring (MAM) begins on March 1, summer (JJA) on June 1, autumn (SON) on September 1, and winter (DJF) on December 1. The seasonal fluxes of t-Al, t-nssCa, and t-Fe for each period are shown as box plots (Fig. 5). The boxes represent the interquartile range (IQR) from the first quartile to the third quartile, and the whiskers indicate the minimum and maximum values within 1.5 times the IQR. Values outside this range are treated as outliers and plotted individually. No clear seasonal patterns are observed in Periods 1 and 2, although Period 1 has slightly higher values in spring and summer. Notably, several high-flux outliers for t-nssCa occur during these seasons in Period 1 (Fig. 5). Periods 3a and 3b exhibit generally similar seasonal patterns, but with some differences in amplitude and variability among seasons. Period 3a shows a slight winter peak across all three elements. In Period 3b, some autumn samples, particularly those from 2013 and 2014, recorded markedly higher fluxes than other seasons, resulting in a wider range in the box plots (Fig. 5). Although the median values of autumn samples are comparable to or lower than those of other seasons, these sporadic high-flux years indicate that enhanced inputs of crustal elements occurred in autumn only during certain years. This suggests that aerosol characteristics in Period 3b were more variable and influenced by episodic dust events in autumn. Amino et al. (2021) reported that dust fluxes in the SE-Dome core were relatively uniform across seasons from 1960 to 1999 but increased significantly in autumn after 2000. The sporadic high autumn fluxes of t-Al, t-nssCa, and t-Fe in Period 3b are broadly consistent with this post-2000 trend, even though they are driven mainly by a few years of strong dust deposition. These seasonal variations in crustal elements further suggest that aerosol compositions differed among periods. The following section discusses the drivers behind the aerosol sources and their associations with dust during each period.

3.4. *Estimation of factors affecting aerosol composition*

The results presented here show that aerosols in the SE-Dome core exhibited different compositions during the three periods. The composition of aerosols in ice cores varies depending on the location and strength of the sources, as well as the atmospheric circulation during transport. Therefore, we estimated the variations in aerosol sources supplying the SE-Dome by comparing the total concentration with the ion and dust data, and discussed the factors affecting these variations in aerosol composition.

In Period 1, the seasonal fluxes of t-Al, t-nssCa, and t-Fe were moderately higher in spring and summer (Fig. 5). Peaks in terrestrial dust and nssCa^{2+} have been observed at many sites across the Greenland ice sheet from late winter to spring (Legrand and Mayewski, 1997; Kuramoto et al., 2011; Oyabu et al., 2016). The chemical and

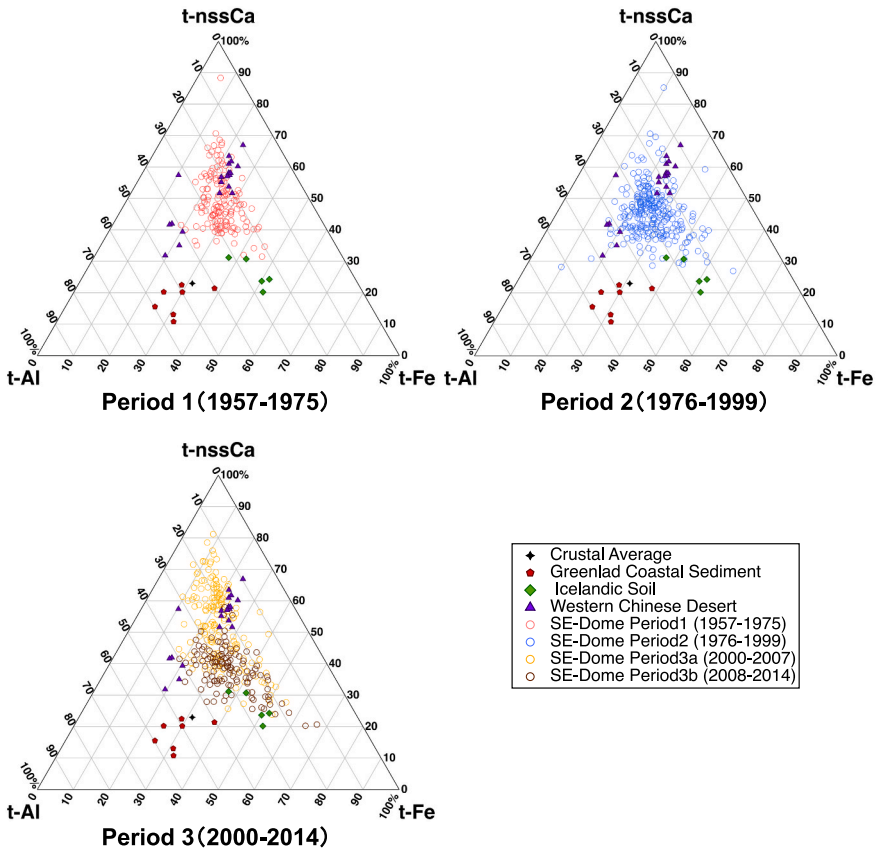

Fig. 4. Comparison of elemental ratios with potential dust source regions. The concentration ratios of t-Al, t-nssCa, and t-Fe in the SE-Dome core by period are compared with the soil composition ratios from potential dust source regions. The data for western China include those from the Taklamakan Desert, Tarim Basin, and Qaidam Basin. References for these regions include Greenland coastal sediments (Loring and Asmund, 1996; Saito, 1998), Icelandic soils (Baldo et al., 2020), Western Chinese deserts (Zhu et al., 2021; Zhao et al., 2019; Makra et al., 2002), and average crustal compositions (Taylor, 1964). These soil composition data are from modern samples and do not correspond to Periods 1–3.

mineralogical compositions of dust deposited in Greenland are predominantly derived from arid regions in Asia (Bory et al., 2003a, 2003b; Drab et al., 2002; Prospero et al., 2002; Fischer et al., 2007), and transport from Asia increases in spring due to frequent dust storms (e.g., Liu et al., 2020). The spring peak in crustal elements in the SE-Dome core may therefore reflect the transport of crustal aerosols from regions in Asia. The ternary diagram shows that Period 1 is enriched in t-nssCa. This plot overlaps with the soil compositions from arid regions in western China, including the Taklamakan Desert, Tarim Basin, and Qaidam Basin (Fig. 4). The median t-nssCa/t-Al and t-Fe/t-Al ratios during Period 1 are 1.95 and 1.09, respectively (Table 4), which fall within the ranges reported for major Asian dust sources (0.31–4.14 and 0.36–1.74; Formenti et al., 2011; Lai et al., 2017).

However, the years of high concentrations of t-Al, t-nssCa, and t-Fe did not coincide with those of dust in Period 1. In particular, the year 1967 showed the highest concentrations of t-Al, t-nssCa, and t-Fe, whereas no corresponding peak was observed in the dust concentration (Fig. 2). This discrepancy may be due to the transport of insoluble particles that are not captured by dust measurements. Amino et al. (2021) measured the dust concentration in the SE-Dome core using a Coulter Counter, which targeted particles between 0.6 and 18 μm in diameter. Consequently, any particles outside this size range, even if supplied, were not included in the dust measurements. Between the 1950s and 1970s, many countries had not yet implemented air pollution controls, and industrial activity and coal combustion were growing, releasing large amounts of greenhouse gases and insoluble particles (e.g., McConnell and Edwards, 2008; Crippa et al., 2016). Major emission sources, such as coal-fired power stations and metal processing facilities, emit fly ash and metal vapors containing Al, Fe, and Ca (Goodarzi, 2006; Lanzerstorfer, 2018). The flux of nssSO_4^{2-} in the SE-Dome core was high during the 1960s–1970s and subsequently declined after 1980, reflecting a decline in anthropogenic SOx emissions from North America (Iizuka et al., 2018). Furthermore, small anthropogenic sulfate particles <0.4 μm are present in samples from the 1970s (Iizuka et al., 2022). The seasonal fluxes of SO_4^{2-} and NO_3^- in the SE-Dome core peak in spring or summer (Iizuka et al., 2018). Although t-Al, t-nssCa, and t-Fe are not necessarily derived from the same sources or supplied at the same times as the ion components, they may reflect anthropogenic aerosol inputs from North America and Europe, which are typically higher in spring and summer. The pronounced peak in 1967, despite no specific emission event being reported, likely reflects increased anthropogenic emissions from industrial activities in these regions.

Period 2 shows seasonal patterns in total metal flux similar to those in Period 1 (Fig. 5). The ternary diagram for Period 2 also overlaps with that for deserts in western China, and the t-nssCa/Al and t-Fe/t-Al ratios are within the range of major Asian sources (Fig. 4; Table 4). However, during Period 2, the concentration significantly decreased (Fig. 2). Significant reductions in dust events from the late 1970s to the 1980s, particularly in the deserts of northern China and East Asia, have been reported (Qian et al., 2002). This decline may reflect a decreased input of Asian dust during Period 2. Furthermore, anthropogenic SOx and NOx emissions are regulated by legislation, including the Clean Air Act enacted in 1963 and amended in 1970 and 1977, with emissions subsequently declining after 1990 (Iizuka et al., 2018; Feng et al., 2020). At least a portion of the decline in total metal concentration between Periods 1 and 2 may be attributed to these reductions in anthropogenic

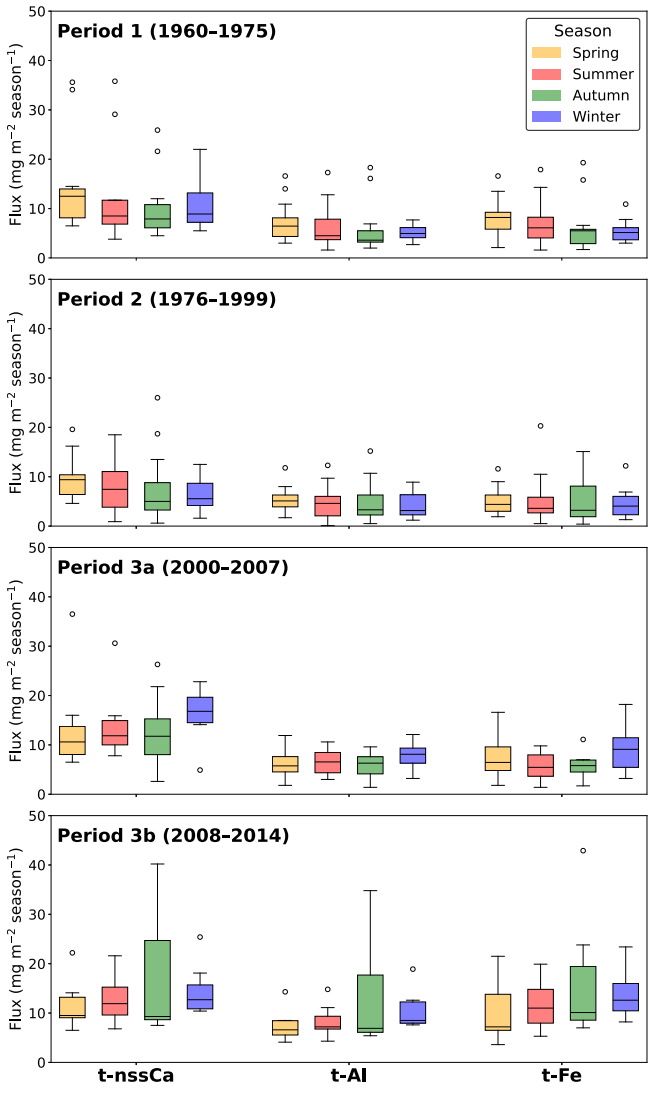

Fig. 5. Box plots of seasonal fluxes (mg m^{-2} season^{-1}) of t-nssCa, t-Al, and t-Fe in the SE-Dome core for each period. The boxes represent the interquartile range (IQR), spanning from the first quartile to the third quartile. The whiskers indicate the minimum and maximum values within 1.5 times the IQR. Values outside this range are considered outliers and are plotted individually. Yellow, red, green, and blue correspond to spring, summer, autumn, and winter, respectively. (For interpretation of the references to colour in this figure legend, the reader is referred to the Web version of this article.)

Table 4
Median and average t-nssCa/t-Al and t-Fe/t-Al ratios for each period in the SE-Dome core.

	t-nssCa/t-Al		t-Fe/t-Al	
	Median	Mean	Median	Mean
Period 1 (1957–1975)	1.95	1.99	1.09	1.12
Period 2 (1976–1999)	1.67	1.65	0.99	1.07
Period 3a (2000–2007)	1.79	2.06	1.02	1.13
Period 3b (2008–2014)	1.52	1.45	1.36	1.31
All Periods (1957–2014)	1.73	1.79	1.09	1.12

emissions.

Period 3 exhibits high total concentrations, dust, and nssCa^{2+} (Figs. 2 and 3). The correlation coefficients between the total concentration and dust concentration are relatively high for all the elements during this period, especially for t-nssCa (r = 0.73; Table 3). This suggests that the total concentration during Period 3 largely reflects inputs from the same sources and transport routes as dust. Amino et al. (2021) suggested that the increase in dust flux in the SE-Dome core after 2000 may be due to a relative increase in coarse dust particles and an increase in their transport from nearby coastal sources in Greenland. Rising temperatures have been observed across much of the Arctic since 2000, including in southeastern Greenland (Bjørk et al., 2012). This warming contributed to glacial retreat and the exposure of previously ice-covered coastal areas (Bendixen et al., 2017; Mouginot et al., 2019), thereby increasing the supply of local dust (Amino et al., 2021). A similar process may have contributed to the increase in total concentration in the SE-Dome core during Period 3; however, its composition exhibits a marked change after 2008 (see Section 3.3). The correlation coefficients between the total concentration and dust concentration varied between Periods 3a and 3b (Table 3). The sources and variation factors for each period are discussed in relation to their aerosol compositions.

Period 3a shows a tendency toward t-nssCa enrichment on a ternary diagram of crustal elements (Fig. 4), with exceptionally high t-nssCa values observed from 2003 to 2005 (Fig. 2). One possible explanation is an increase in soluble nssCa. Based on back trajectory analysis, Amino et al. (2021) identified the 65–75°N section of Greenland's east coast as a likely source and reported an expansion of snow-free areas there after 2000. In various coastal regions of Greenland, glacial meltwater lakes and streams are present, often exhibiting high concentrations of soluble Ca^{2+} and Mg^{2+} (Auqué et al., 2019). Some exposed bedrock in these areas consists of dolomite, represented as $CaMg(CO_3)_2$ (Geological Survey of Denmark and Greenland, 2005), which typically contains abundant Ca^{2+} (Drits et al., 2005). In addition, Period 3a exhibited elevated dust concentrations (Fig. 2), indicating increased inputs not only of soluble nssCa but also of insoluble particles. Southern and eastern Greenland are dominated by Precambrian metamorphic rocks and granite, which are rich in Fe and Al but poor in Ca (Kolb et al., 2016). In contrast, limestone and dolomite sediments are found along the western coast and in northeastern basin areas (Geological Survey of Denmark and Greenland, 2005; Salomon et al., 2020). Glacial retreat may have exposed these carbonate rocks, promoting their weathering and contributing Ca-rich aerosols to the SE-Dome. Some autumn samples during Period 3b, showed elevated fluxes of t-Al, t-nssCa, and t-Fe (Fig. 5). These episodic increases are broadly consistent with the post-2000 trend of enhanced autumn dust fluxes reported for the SE-Dome core (Amino et al., 2021). The autumn increase in dust flux observed in the SE-Dome core has been attributed to delayed seasonal snowfall along the Greenland coast due to rising temperatures, which expand snow-free areas. The elevated fluxes observed in this study may similarly reflect enhanced local dust input from the Greenland coast during those specific years.

The correlations between the t-Al, t-nssCa, t-Fe concentrations, and coarse dust (>5 μm) concentrations were weak from Periods 1 to 3a but moderate during Period 3b (r = 0.57 for t-Al, r = 0.50 for t-nssCa; Table 5). Although not statistically significant ($p > 0.05$) due to small sample sizes, these stronger correlations in Period 3b support increased dust input from local sources. The compositional ratios of the three crustal elements during Periods 1 to 3a are enriched in t-nssCa, matching

Table 5
Correlation coefficients between >5 μm dust concentration (Amino et al., 2021) and t-Al, t-nssCa, and t-Fe in the SE-Dome core for each period (1960–2014). The sample size (number of years) for each period is indicated by n.

	t-Al	t-nssCa	t-Fe	n
Period 1 (1957–1975)	0.17^{+}	0.19^{+}	0.26^{+}	16
Period 2 (1976–1999)	−0.18^{+}	−0.07^{+}	−0.03^{+}	24
Period 3a (2000–2007)	0.36^{+}	0.09^{+}	0.02^{+}	8
Period 3b (2008–2014)	0.57^{+}	0.50^{+}	0.36^{+}	7
All Periods (1957–2014)	0.29$^{\#}$	0.36*	0.31$^{\#}$	55

$^{+}$ $p > 0.05$, $^{\#}$ $0.05 > p > 0.01$, * $0.01 > p > 0.001$.

the composition of desert regions in western China. However, in Period 3b, samples with more than 50 % t-nssCa became rare, whereas those enriched in t-Fe increased (Fig. 4). This compositional shift likely reflects changes in the intensity or contribution of different sources. The disappearance of t-nssCa enrichment in Period 3 may be explained by an increased local dust supply from Greenland, which relatively reduced contributions from Asian arid regions. This is supported by the compositional ratios falling between those of the western Chinese deserts and the Greenland coastal region (Fig. 4). Previous studies have shown a decreasing trend in Asian dust intensity from approximately 1980 to 2020 (Nagashima et al., 2016; Liu et al., 2020), suggesting that reduced input from Asian arid regions may have contributed to the compositional change in SE-Dome aerosols. Samples enriched in t-Fe were also observed during Period 3b (Fig. 4). Volcanic soils derived from basaltic rocks represent a potential source of Fe-rich aerosols. Icelandic andosol, a volcanic ash-derived soil, contains high Fe_2O_3 (10–15 wt%) and moderate amounts of Al_2O_3 and CaO, reflecting its volcanic origin (Baldo et al., 2020). The compositional ratios of the three crustal elements in the SE-Dome core during Period 3b overlap with those of Icelandic soil (Fig. 4). This suggests that Fe-rich aerosols may have been transported from Iceland to the SE-Dome during this period.

In summary, Period 3 featured an increase in the local dust supply from the Greenland coastal region alongside a relative decrease in the input from Asian arid regions. The compositional differences between Periods 3a and 3b likely reflect these changes in source contributions. Supplementary inputs from Iceland may also have contributed during this period.

4. Conclusions

This study measured the total concentrations of four major metal elements (Na, Al, Ca, and Fe) in an ice core from SE-Dome, southeastern Greenland, and reconstructed their temporal variations from 1957 to 2014. The results show that the crustal elements (t-Al, t-nssCa, and t-Fe) exhibit similar variation patterns, with high concentrations during 1957–1975 (Period 1), low concentrations during 1976–1999 (Period 2), and a subsequent increase after 2000 (Period 3). These pronounced concentration variations served as the basis for defining the three periods and identifying the factors that affected their respective concentration trends.

The compositional ratios of t-Al, t-nssCa, and t-Fe did not differ significantly between Periods 1 and 2. However, Period 3 exhibited a shift: the earlier half (Period 3a, before 2008) was enriched in t-nssCa, whereas the latter half (Period 3b, after 2008) tended toward higher t-Fe. The seasonal mean fluxes of these three elements peaked in spring and summer during Period 1, whereas in some years of Period 3b, elevated fluxes were observed in autumn. These differences in elemental ratios and seasonal trends across the periods suggest variations in aerosol composition. The high concentrations of t-Al, t-nssCa, and t-Fe during Period 1, with peaks in spring, likely reflect inputs of dust from arid regions in Asia. In addition, the discrepancy between dust and total concentration trends may indicate contributions from anthropogenic aerosols originating in North America and Europe. The marked decrease in concentrations during Period 2 may be attributed not only to reduced dust transport from Asian deserts but also to declines in anthropogenic emissions due to air pollution regulations. An increased influence from local Greenlandic sources characterizes period 3. The t-nssCa-enriched composition of Period 3a likely resulted from elevated soluble $nssCa^{2+}$ concentrations in meltwater from rivers and lakes along the Greenland coast, as well as from weathering products of carbonate rocks newly exposed by glacial retreat. In Period 3b, greater contributions from local Greenland soil led to a relative decline in dust transported from Asia, resulting in an intermediate elemental composition. The presence of Fe-rich compositions also suggests the possibility of additional aerosol input from volcanic soils in Iceland.

This study analyzed total metal concentrations, including both soluble and insoluble fractions, revealing aerosol inputs and potential changes in their sources that were not fully captured by conventional ion or dust concentration data alone. These results highlight the importance of identifying the composition of insoluble particles. Although total metal concentrations allow for a more detailed estimation of aerosol sources, they do not provide definitive identification, as achieved through isotope ratio analyses of Sr, Nd, and Pb. However, the significance of this study lies in integrating previously independent discussions of dust and ion concentrations to reconstruct the entire aerosol load, including both components quantitatively. Future studies that incorporate total metal concentrations, along with fundamental analyses of ions and dust, and interpret these data together will help strengthen and refine reconstructions of past climate and environmental changes using aerosols. The present results may also serve as a basis for improving chemistry transport models, particularly by providing constraints on how local emissions are represented.

CRediT authorship contribution statement

Nao Esashi: Writing – original draft, Visualization, Investigation, Formal analysis, Data curation. **Chiaki Sasaki:** Investigation, Formal analysis, Data curation. **Toshitaka Suzuki:** Validation, Supervision, Methodology, Investigation, Funding acquisition, Data curation, Conceptualization. **Motohiro Hirabayashi:** Validation, Investigation, Data curation. **Yoshinori Iizuka:** Writing – review & editing, Supervision, Project administration, Investigation, Funding acquisition, Conceptualization. **Sumito Matoba:** Investigation. **Koji Fujita:** Writing – original draft, Supervision.

Declaration of competing interest

The authors declare that they have no known competing financial interests or personal relationships that could have appeared to influence the work reported in this paper.

Acknowledgments

We are grateful to the drilling and initial analysis teams of the SE-Dome ice core project. This study was supported by JSPS-KAKENHI (Grants 18H05292 and 26257201), the Grant for Joint Research Program of the Institute of Low Temperature Science, Hokkaido University, and the General Collaboration Project of the National Institute of Polar Research. This work was partially carried out in the Arctic Challenge for Sustainability (ArCS and ArCS II) Project, Program Grant Number JPMXD1420318865. The data used in this study is available in the Zenodo (https://doi.org/10.5281/zenodo.17349018).

References

Amino, T., Iizuka, Y., Matoba, S., Shimada, R., Oshima, N., Suzuki, T., Ando, T., Aoki, T., Fujita, K., 2021. Increasing dust emission from ice free terrain in southeastern Greenland since 2000. Polar Science 27, 100599. https://doi.org/10.1016/j.polar.2020.100599.

Auqué, L.F., Puigdomenech, I., Tullborg, E.-L., Gimeno, M.J., Grodzinsky, K., Hogmalm, K.J., 2019. Chemical weathering in a moraine at the ice sheet margin at Kangerlussuaq, western Greenland. Arctic Antarct. Alpine Res. 51 (1), 440–459. https://doi.org/10.1080/15230430.2019.1660125.

Baldo, C., Formenti, P., Nowak, S., Chevaillier, S., Cazaunau, M., Pangui, E., Di Biagio, C., Doussin, J.-F., Ignatyev, K., Dagsson-Waldhauserova, P., Arnalds, O., MacKenzie, A.R., Shi, Z., 2020. Distinct chemical and mineralogical composition of Icelandic dust compared to northern African and Asian dust. Atmos. Chem. Phys. 20 (21), 13521–13539. https://doi.org/10.5194/acp-20-13521-2020.

Banta, J.R., McConnell, J.R., Edwards, R., Engelbrecht, J.P., 2008. Delineation of carbonate dust, aluminous dust, and sea salt deposition in a Greenland glaciochemical array using positive matrix factorization. G-cubed 9 (7). https://doi.org/10.1029/2007GC001908.

Bendixen, M., Lønsmann Iversen, L., Anker Bjørk, A., Elberling, B., Westergaard-Nielsen, A., Overeem, I., Barnhart, K.R., Abbas Khan, S., Box, J.E., Abermann, J., Langley, K., Kroon, A., 2017. Delta progradation in Greenland driven by increasing glacial mass loss. Nature 550 (7674), 101–104. https://doi.org/10.1038/nature23873.

Bjørk, A.A., Kjær, K.H., Korsgaard, N.J., Khan, S.A., Kjeldsen, K.K., Andresen, C.S., Box, J. E., Larsen, N.K., Funder, S., 2012. An aerial view of 80 years of climate-related glacier fluctuations in southeast Greenland. Nat. Geosci. 5 (6), 427–432. https://doi.org/10.1038/ngeo1481.

Bory, A.J.-M., Biscaye, P.E., Grousset, F.E., 2003a. Two distinct seasonal Asian source regions for mineral dust deposited in Greenland (NorthGRIP). Geophys. Res. Lett. 30 (4). https://doi.org/10.1029/2002GL016446.

Bory, A.J.-M., Biscaye, P.E., Piotrowski, A.M., Steffensen, J.P., 2003b. Regional variability of ice core dust composition and provenance in Greenland. G-cubed 4 (12). https://doi.org/10.1029/2003GC000627.

Broecker, W.S., Peng, T.-H., 1982. Tracers in the Sea. The Lamont-Doherty Geological Observatory, Columbia University, Palisades, New York.

Crippa, M., Janssens-Maenhout, G., Dentener, F., Guizzardi, D., Sindelarova, K., Muntean, M., Dingenen, R.V., Granier, C., 2016. Forty years of improvements in European air quality: regional policy-industry interactions with global impacts. Atmos. Chem. Phys. 16, 3825–3841. https://doi.org/10.5194/acp-16-3825-2016.

de Caritat, P., Hall, G., Gíslason, S., Belsey, W., Braun, M., Goloubeva, N.I., Olsen, H.K., Scheie, J.O., Vaive, J.E., 2005. Chemical composition of arctic snow: concentration levels and regional distribution of major elements. Sci. Total Environ. 336 (1–3), 183–199. https://doi.org/10.1016/j.scitotenv.2004.05.031.

Dibb, J.E., Whitlow, S.I., Arsenault, M., 2007. Seasonal variations in the soluble ion content of snow at Summit, Greenland: constraints from three years of daily surface snow samples. Atmos. Environ. 41 (24), 5007–5019. https://doi.org/10.1016/j.atmosenv.2006.12.010.

Drab, E., Gaudichet, A., Jaffrezo, J.L., Colin, J.L., 2002. Mineral particles content in recent snow at Summit (Greenland). Atmos. Environ. 36 (34), 5365–5376. https://doi.org/10.1016/s1352-2310(02)00470-3.

Drits, V.A., McCarty, D.K., Sakharov, B., Milliken, K.L., 2005. New insight into structural and compositional variability in some ancient excess-Ca dolomite. Can. Mineral. 43 (4), 1255–1290. https://doi.org/10.2113/gscanmin.43.4.1255.

Feng, J., Chan, E., Vet, R., 2020. Air quality in the eastern United States and Eastern Canada for 1990–2015: 25 years of change in response to emission reductions of SO_2 and NO_x in the region. Atmos. Chem. Phys. 20, 3107–3134. https://doi.org/10.5194/acp-20-3107-2020.

Fischer, H., Siggaard-Andersen, M.-L., Ruth, U., Röthlisberger, R., Wolff, E., 2007. Glacial/interglacial changes in mineral dust and sea-salt records in polar ice cores: sources, transport, and deposition. Rev. Geophys. 45 (1). https://doi.org/10.1029/2005RG000192.

Formenti, P., Schütz, L., Balkanski, Y., Desboeufs, K., Ebert, M., Kandler, K., Zhang, D., 2011. Recent progress in understanding physical and chemical properties of African and Asian mineral dust. Atmos. Chem. Phys. 11 (16), 8231–8256. https://doi.org/10.5194/acp-11-8231-2011.

Furukawa, R., Uemura, R., Fujita, K., Sjolte, J., Yoshimura, K., Matoba, S., Iizuka, Y., 2017. Seasonal-scale dating of a shallow ice core from Greenland using oxygen isotope matching between data and simulation. J. Geophys. Res. Atmos. 122 (20), 10873–10887. https://doi.org/10.1002/2017JD026716.

Gaspari, V., Barbante, C., Cozzi, G., Cescon, P., Boutron, C.F., Gabrielli, P., Capodaglio, G., Ferrari, C., Petit, J.R., Delmonte, B., 2006. Atmospheric iron fluxes over the last deglaciation: climatic implications. Geophys. Res. Lett. 33 (3). https://doi.org/10.1029/2005GL024352.

Geological Survey of Denmark and Greenland, 2005. Geology of Greenland, vol. 185. Geological Survey of Denmark and Greenland Bulletin. https://eng.geus.dk/media/14258/nr185_p24-52.pdf.

Ghermandi, G., Cecchi, R., Capotosto, M., Marino, F., 2003. Elemental composition determined by PIXE analysis of the insoluble aerosol particles in EPICA-Dome C ice core samples representing the last 27000 years. Geophys. Res. Lett. 30 (22). https://doi.org/10.1029/2003GL018169.

Goodarzi, F., 2006. Characteristics and composition of fly ash from Canadian coal-fired power plants. Fuel 85 (10–11), 1418–1427. https://doi.org/10.1016/j.fuel.2005.11.022.

Iizuka, Y., Matoba, S., Yamasaki, T., Oyabu, I., Kadota, M., Aoki, T., 2016. Glaciological and meteorological observations at the SE-Dome site, southeastern Greenland Ice sheet. Bull. Glaciol. Res. 34 (0), 1–10. https://doi.org/10.5331/bgr.15r03.

Iizuka, Y., Miyamoto, A., Hori, A., Matoba, S., Furukawa, R., Saito, T., Fujita, S., Hirabayashi, M., Yamaguchi, S., Fujita, K., Takeuchi, N., 2017. A firn densification process in the high accumulation dome of southeastern Greenland. Arctic Antarct. Alpine Res. 49 (1), 13–27. https://doi.org/10.1657/aaar0016-034.

Iizuka, Y., Uemura, R., Fujita, K., Hattori, S., Seki, O., Miyamoto, C., Suzuki, T., Yoshida, N., Motoyama, H., Matoba, S., 2018. A 60 year record of atmospheric aerosol depositions preserved in a high-accumulation dome ice core, southeast Greenland. J. Geophys. Res. Atmos. 123 (1), 574–589. https://doi.org/10.1002/2017jd026733.

Iizuka, Y., Uemura, R., Matsui, H., Oshima, N., Kawakami, K., Hattori, S., Ohno, H., Matoba, S., 2022. High flux of small sulfate aerosols during the 1970s reconstructed from the SE-dome ice core in Greenland. J. Geophys. Res. Atmos. 127 (17). https://doi.org/10.1029/2022jd036880.

Kjær, H.A., Zens, P., Black, S., Lund, K.H., Svensson, A., Vallelonga, P., 2022. Canadian forest fires, Icelandic volcanoes and increased local dust observed in six shallow Greenland firn cores. Clim. Past 18 (10), 2211–2230. https://doi.org/10.5194/cp-18-2211-2022.

Kolb, J., Stensgaard, B.M., Kokfelt, T.F. (Eds.), 2016. Geology and Mineral Potential of South-East Greenland, 2016/38. Geological Survey of Denmark and Greenland Report. https://data.geus.dk/g500segment/32459_GEUS-R_2016_38.pdf.

Komuro, Y., Nakazawa, F., Goto-Azuma, K., Hirabayashi, M., Shigeyama, W., Fujita, K., Steffensen, J.P., Dahl-Jensen, D., 2024. Major metallic elements (Al, Ca, and Fe) and size distribution of mineral particles in recent snow in inland Northeast Greenland. Bull. Glaciol. Res. 42, 49–60. https://doi.org/10.5331/bgr.24a02.

Krnavek, L., Simpson, W.R., Carlson, D., Domine, F., Douglas, T.A., Sturm, M., 2012. The chemical composition of surface snow in the Arctic: examining marine, terrestrial, and atmospheric influences. Atmos. Environ. 50, 349–359. https://doi.org/10.1016/j.atmosenv.2011.11.033.

Kuramoto, T., Goto-Azuma, K., Hirabayashi, M., Miyake, T., Motoyama, H., Dahl-Jensen, D., Steffensen, J.P., 2011. Seasonal variations of snow chemistry at NEEM, Greenland. Ann. Glaciol. 52 (58), 193–200. https://doi.org/10.3189/172756411797252365.

Lai, A.M., Shafer, M.M., Dibb, J.E., Polashenski, C.M., Schauer, J.J., 2017. Elements and inorganic ions as source tracers in recent Greenland snow. Atmos. Environ. 164, 205–215. https://doi.org/10.1016/j.atmosenv.2017.05.048.

Lanzerstorfer, C., 2018. Fly ash from coal combustion: dependence of the concentration of various elements on the particle size. Fuel 228, 263–271. https://doi.org/10.1016/j.fuel.2018.04.136.

Legrand, M., Mayewski, P.A., 1997. Glaciochemistry of polar ice cores: a review. Rev. Geophys. 35 (3), 219–243. https://doi.org/10.1029/96RG03527.

Liu, J., Wu, D., Liu, G., Mao, R., Chen, S., Ji, M., Fu, P., Sun, Y., Pan, X., Jin, H., Zhou, Y., Wang, X., 2020. Impact of Arctic amplification on declining spring dust events in East Asia. Clim. Dyn. 54 (3–4), 1913–1935. https://doi.org/10.1007/s00382-019-05094-4.

Loring, D.H., Asmund, G., 1996. Geochemical factors controlling accumulation of major and trace elements in Greenland coastal and fjord sediments. Environ. Geol. 28 (1), 2–11. https://doi.org/10.1007/s002540050072.

Lupker, M., Aciego, S.M., Bourdon, B., Schwander, J., Stocker, T.F., 2010. Isotopic tracing (Sr, Nd, U and Hf) of continental and marine aerosols in an 18th century section of the Dye-3 ice core (Greenland). Earth Planet Sci. Lett. 295 (1–2), 277–286. https://doi.org/10.1016/j.epsl.2010.04.010.

Makra, L., Borbély-Kiss, I., Koltay, E., Chen, Y., 2002. Enrichment of desert soil elements in Takla Makan dust aerosol. Nucl. Instrum. Methods Phys. Res. Sect. B Beam Interact. Mater. Atoms 189 (1–4), 214–220. https://doi.org/10.1016/s0168-583x(01)01045-x.

Marino, F., Maggi, V., Delmonte, B., Ghermandi, G., Petit, J.R., 2004. Elemental composition (Si, Fe, Ti) of atmospheric dust over the last 220 kyr from the EPICA ice core (Dome C, Antarctica). Ann. Glaciol. 39, 110–118. https://doi.org/10.3189/172756404781813862.

McConnell, J.R., Edwards, R., 2008. Coal burning leaves toxic heavy metal legacy in the Arctic. Proc. Natl. Acad. Sci. U. S. A 105 (34), 12140–12144. https://doi.org/10.1073/pnas.0803564105.

Miyamoto, C., Iizuka, Y., Matoba, S., Hattori, S., Takahashi, Y., 2022. Gypsum formation from calcite in the atmosphere recorded in aerosol particles transported and trapped in Greenland ice core sample is a signature of secular change of SO2 emission in East Asia. Atmos. Environ. 278 (119061), 119061. https://doi.org/10.1016/j.atmosenv.2022.119061.

Mouginot, J., Rignot, E., Bjørk, A.A., van den Broeke, M., Millan, R., Morlighem, M., Noël, B., Scheuchl, B., Wood, M., 2019. Forty-six years of Greenland Ice sheet mass balance from 1972 to 2018. Proc. Natl. Acad. Sci. U. S. A 116 (19), 9239–9244. https://doi.org/10.1073/pnas.1904242116.

Nagashima, K., Suzuki, Y., Irino, T., Nakagawa, T., Tada, R., Hara, Y., Yamada, K., Kurosaki, Y., 2016. Asian dust transport during the last century recorded in Lake Suigetsu sediments. Geophys. Res. Lett. 43, 2835–2842. https://doi.org/10.1002/2015GL067589.

Nagatsuka, N., Goto-Azuma, K., Tsushima, A., Fujita, K., Matoba, S., Onuma, Y., Dallmayr, R., Kadota, M., Hirabayashi, M., Ogata, J., Ogawa-Tsukagawa, Y., Kitamura, K., Minowa, M., Komuro, Y., Motoyama, H., Aoki, T., 2021. Variations in mineralogy of dust in an ice core obtained from northwestern Greenland over the past 100 years. Clim. Past 17, 1341–1362. https://doi.org/10.5194/cp-17-1341-2021.

Nakazawa, F., Nagatsuka, N., Hirabayashi, M., Goto-Azuma, K., Steffensen, J.P., Dahl-Jensen, D., 2021. Variation in recent annual snow deposition and seasonality of snow chemistry at the east Greenland ice core project (EGRIP) camp, Greenland. Polar Science 27 (100597), 100597. https://doi.org/10.1016/j.polar.2020.100597.

Oyabu, I., Matoba, S., Yamasaki, T., Kadota, M., Iizuka, Y., 2016. Seasonal variations in the major chemical species of snow at the South East Dome in Greenland. Polar Science 10 (1), 36–42. https://doi.org/10.1016/j.polar.2016.01.003.

Prospero, J.M., Ginoux, P., Torres, O., Nicholson, S.E., Gill, T.E., 2002. Environmental characterization of global sources of atmospheric soil dust identified with the Nimbus 7 total ozone mapping spectrometer (TOMS) absorbing aerosol product. Rev. Geophys. 40 (1). https://doi.org/10.1029/2000RG000095, 2-1–2-31.

Qian, W., Quan, L., Shi, S., 2002. Variations of the dust storm in China and its climatic control. J. Clim. 15 (10), 1216–1229. https://doi.org/10.1175/1520-0442(2002)015<1216:votdsi>2.0.co, 2.

Ruth, U., Barbante, C., Bigler, M., Delmonte, B., Fischer, H., Gabrielli, P., Gaspari, V., Kaufmann, P., Lambert, F., Maggi, V., Marino, F., Petit, J.-R., Udisti, R., Wagenbach, D., Wegner, A., Wolff, E.W., 2008. Proxies and measurement techniques for mineral dust in Antarctic ice cores. Environ. Sci. Technol. 42 (15), 5675–5681. https://doi.org/10.1021/es703078z.

Ruth, U., Wagenbach, D., Bigler, M., Steffensen, J.P., Röthlisberger, R., Miller, H., 2002. High-resolution microparticle profiles at NorthGRIP, Greenland: case studies of the calcium–dust relationship. Ann. Glaciol. 35, 237–242. https://doi.org/10.3189/172756402781817347.

Saito, S., 1998. Major and trace element geochemistry of sediments from East Greenland Continental rise: an implication for sediment provenance and source area weathering. Proc. Ocean Drill. Progr. Sci. Results 152. https://doi.org/10.2973/odp.proc.sr.152.207.1998.

Salomon, E., Rotevatn, A., Kristensen, T.B., Grundvåg, S.-A., Henstra, G.A., Meckler, A. N., Albert, R., Gerdes, A., 2020. Fault-controlled fluid circulation and diagenesis along basin-bounding fault systems in rifts–insights from the East Greenland rift system. Solid Earth 11, 1987–2013. https://doi.org/10.5194/se-11-1987-2020.

Sato, H., Suzuki, T., Hirabayashi, M., Iizuka, Y., Motoyama, H., Fujii, Y., 2013. Mineral and sea-salt aerosol fluxes over the last 340 kyr reconstructed from the total concentration of Al and Na in the Dome Fuji ice core. Atmos. Clim. Sci. 3 (2), 186–192. https://doi.org/10.4236/acs.2013.32020.

Schüpbach, S., Fischer, H., Bigler, M., Erhardt, T., Gfeller, G., Leuenberger, D., Mini, O., Mulvaney, R., Abram, N.J., Fleet, L., Frey, M.M., Thomas, E., Svensson, A., Dahl-Jensen, D., Kettner, E., Kjaer, H., Seierstad, I., Steffensen, J.P., Rasmussen, S.O., Wolff, E.W., 2018. Greenland records of aerosol source and atmospheric lifetime changes from the Eemian to the Holocene. Nat. Commun. 9 (1), 1476. https://doi.org/10.1038/s41467-018-03924-3.

Steffensen, J.P., 1997. The size distribution of microparticles from selected segments of the Greenland Ice core project ice core representing different climatic periods. J. Geophys. Res. Oceans 102 (C12), 26755–26763. https://doi.org/10.1029/97JC01490.

Suzuki, T., Sensui, M., 1991. Application of the microwave acid digestion method to the decomposition of rock samples. Anal. Chim. Acta 245, 43–48. https://doi.org/10.1016/s0003-2670(00)80199-3.

Taylor, S.R., 1964. Abundance of chemical elements in the continental crust: a new table. Geochem. Cosmochim. Acta 28 (8), 1273–1285. https://doi.org/10.1016/0016-7037(64)90129-2.

Wei, Z., Hattori, S., Tsuruta, A., Jiang, Z., Ishino, S., Fujita, K., Iizuka, Y., 2025. A 60-year atmospheric nitrate isotope record from a southeastern Greenland ice core with minimal postdepositional alteration. Atmos. Chem. Phys. 25 (11), 5727–5742. https://doi.org/10.5194/acp-25-5727-2025.

Whitlow, S., Mayewski, P.A., Dibb, J.E., 1992. A comparison of major chemical species seasonal concentration and accumulation at the South pole and summit, Greenland. Atmos. Environ. 26 (11), 2045–2054. https://doi.org/10.1016/0960-1686(92)90089-4.

Zhao, W., Liu, L., Chen, J., Ji, J., 2019. Geochemical characterization of major elements in desert sediments and implications for the Chinese loess source. Sci. China Earth Sci. 62 (9), 1428–1440. https://doi.org/10.1007/s11430-018-9354-y.

Zhu, B.-Q., Zhang, J.-X., Sun, C., 2021. Physiochemical characteristics, provenance, and dynamics of sand dunes in the arid Hexi Corridor. Front. Earth Sci. 9. https://doi.org/10.3389/fear.